

Particulate and mineral-associated organic carbon turnover revealed by modelling their long-term dynamics

Xiaowei Guo^a, Raphael A. Viscarra Rossel^b, Guocheng Wang^c, Liujun Xiao^a, Mingming Wang^a, Shuai Zhang^a, Zhongkui Luo^{a,d,e,*}

^a College of Environmental and Resource Sciences, Zhejiang University, Hangzhou, Zhejiang, 310058, China

^b Soil & Landscape Science, School of Molecular and Life Sciences, Curtin University, GPO Box U1987, Perth, WA, 6845, Australia

^c LAPC, Institute of Atmospheric Physics, Chinese Academy of Sciences, Beijing, 100029, China

^d Academy of Ecological Civilization, Zhejiang University, Hangzhou, 310058, China

^e Key Laboratory of Environment Remediation and Ecological Health, Ministry of Education, Zhejiang University, Hangzhou, 310058, China



ARTICLE INFO

Keywords:

Functional carbon fractions
Soil carbon model
Carbon turnover
Parameter identifiability
Uncertainty
Model complexity

ABSTRACT

Particulate (POC) and mineral-associated organic carbon (MOC) are measurable carbon pools with distinct function. Their turnover properties have been rarely assessed because of their contrasting stabilization and destabilization processes and the difficulty of *in situ* monitoring. In this study we used two carbon models (a three-pool and a four-pool model) driven by measured POC, MOC and a more resistant charred organic carbon (COC) pool to obtain insights into the turnover of POC and MOC and to predict long-term soil organic carbon (SOC) dynamics. The models were constrained by measurements of POC, MOC and COC at 159 long-term trials (average trial duration is 22 years) across Australian agricultural regions. Results showed that POC-, MOC- and COC-constrained models, particularly the three-pool model, have less parameter collinearity and predict less uncertainties in most model parameters as well as in SOC dynamics and its vulnerability, compared with the models constrained by total SOC alone. The three-pool model estimated an average decay rate of 0.46 and 0.044 yr^{-1} for POC and MOC, respectively, across the trials. The four-pool model provided additional insights that on average a large fraction of MOC (28% on average across the trials) is physically protected against decomposition, and the remaining fraction is labile with an average decay rate of 0.068 yr^{-1} . The existence of protected MOC results in prolonged overall residence time of MOC. Additionally, we found that the turnover of POC and MOC are distinctly influenced by climate and soil properties with involvement of non-linear relationships. These results shed new lights on the dynamics of measurable functional SOC pools and demonstrate that models constrained by these pools can provide more accurate predictions of model parameters thereby more accurate projections of SOC dynamics compared to models constrained by total SOC only.

1. Introduction

Soil organic carbon (SOC) is an indicator of soil health (Lal, 2016), and increase of SOC stock not only mitigates climate change (Paustian et al., 2016) but also improves soil functionality (e.g., soil fertility and thus agricultural productivity) (Lal, 2004; Wiesmeier et al., 2019). For effective SOC sequestration and management, SOC models are a common tool for making SOC predictions and guiding policy. A large number of models such as RothC (Jenkinson and Rayner, 1977), Century (Parton et al., 1988), ICBM (Andrén and Kätterer, 1997) have been developed, and SOC pools are the basis of these SOC models (Luo et al.,

2016; Sulman et al., 2018). Generally, in these models SOC is divided into several conceptual pools that are simulated by first-order kinetics. Pool sizes and their turnover are crucial to correctly simulate SOC dynamics but are usually empirically derived for model initialization, without explicit consideration of the mechanisms underpinning their turnover or transfer between different pools. To overcome these challenges, using measured SOC fractions has been proposed (Smith et al., 2002), which try to link conceptual SOC pools to their measurable counterparts (Skjemstad et al., 2004; Zimmermann et al., 2007; Lee and Viscarra Rossel, 2020). Nonetheless, the potential distinct turnover behaviours of the measured fractions and underlying controls (Luo et al.,

01

mingxi zhang

* Corresponding author. College of Environmental and Resource Sciences, Zhejiang University, Hangzhou, Zhejiang, 310058, China.

E-mail address: luozk@zju.edu.cn (Z. Luo).

2020; Lugato et al., 2021) have been rarely considered in relevant model applications.

02 Emerging conceptualization of functionally contrasting SOC pools considers their specific stabilization and destabilization mechanisms (Cotrufo et al., 2019; Viscarra Rossel et al., 2019; Luo et al., 2020; Lugato et al., 2021). Lavallee et al. (2020) recommended the separation of SOC to two such pools: particulate (POC) and mineral-associated organic carbon (MOC), and detailed the fundamentally contrasting mechanisms underpinning their formation, persistence and function. In brief, POC is mainly comprised of fragments of plant materials (undecomposed or partially decomposed), nutrient-poor, and has a customary particle size of >53 µm, while MOC mainly consists of microbial- and plant-origin with low molecular weight, relatively nutrient-rich, and has a customary particle size of <53 µm. Another fundamental difference is that MOC can be physically protected from decomposition via association with soil minerals, but POC cannot. That means microbes can only use free MOC that is dissociated from minerals. For these reasons, POC and MOC would present distinct turnover behaviours and responses to climate and environmental changes. By synthesising European-wide measurements of POC and MOC, indeed, Lugato et al. (2021) found that POC and MOC show different vulnerability to climate change. One of our previous studies using temporal measurements of POC and MOC in Australian agricultural regions also found that POC and MOC show distinct temporal dynamics in response to land use changes (Luo et al., 2020). However, the detailed turnover properties such as decay rates of POC and MOC, physical protection processes underpinning MOC stabilization/destabilization and their environmental controls have not been quantitatively assessed. The primary barrier is the lack of long-term data sets and the difficulty to directly measure those processes in situ. Without this information, it would be difficult to obtain reliable SOC predictions to identify suitable management practices for long-term carbon sequestration. Integrating state-of-the-art knowledge of the functionally distinct POC and MOC fractions and relevant temporal measurements into process-based SOC modelling would improve our confidence on SOC predictions and deepen our understanding of POC and MOC turnover.

03 In this study, we used two SOC models primarily driven by temporal measurements of POC, MOC and COC (Fig. 1). The three-pool model (M3) generally follows the same structure of ICBM (Andrén and Kätterer, 1997), treating POC, MOC and COC as three distinct pools, and the dynamics of POC and MOC are simulated as a first-order decay process and COC is treated as a resistant pool (Fig. 1a). In the four-pool model (M4), MOC is further divided into labile MOC (MOC_l , which is readily available for decomposition) and protected MOC (MOC_p , which is physically protected against decomposition, Fig. 1b) to acknowledge the importance of physical protection in MOC dynamics, and the transfer between MOC_p and MOC_l is simulated as a dynamic adsorption-desorption process (Fig. 1b). Our aim was to demonstrate the importance of modelling functionally distinct SOC pools and bring relevant insights into the understanding of the turnover processes underpinning POC and MOC dynamics. The two models (M3 vs M4) also allow us to assess how model structure/complexity influences the estimation of model parameters and prediction accuracy.

2. Materials and methods

2.1. Soil carbon dataset

The legacy data collected from 176 trials at 74 sites across Australian agricultural regions (Skjemstad and Spounger, 2003) were used. In this study, only the trials with experimental duration of longer than five years included (159 trials at 69 sites, Fig. S1). These trials cover important agricultural management (e.g., cereal croplands, pasture and pasture-crop rotations) and agro-ecological regions in Australia with an average trial duration of 22 years. A detailed description about the trials and data can be found in Skjemstad and Spounger (2003).

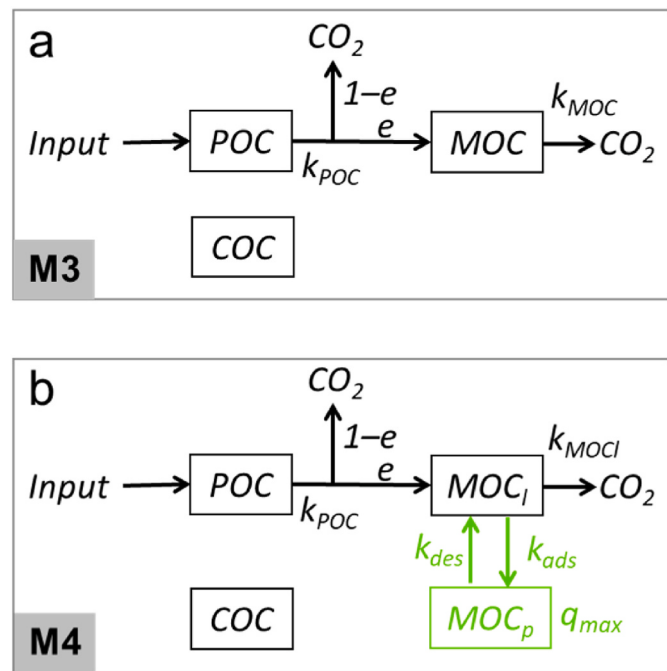


Fig. 1. Diagram of two models driven by functionally distinct soil carbon fractions. (a) M3 simulates three carbon pools (i.e., POC, MOC and COC). (b) M4 simulates four carbon pools and divides MOC into labile fraction readily available for decomposition (MOC_l) and protected fraction against decomposition (MOC_p), and the dynamics of MOC_l and MOC_p are simulated as a dynamic adsorption (k_{ads}) and desorption (k_{des}) process. Charred organic carbon (COC) is assumed to be resistant to decomposition and treated as a constant in both models. See Table 1 for the details of model parameters.

For each trial, aboveground plant residues (Mg dry mass $ha^{-1} yr^{-1}$) retained was recorded for each experimental year and converted to carbon using a factor of 0.45. At each time point of measurements, soil cores (up to 80 cores depending on trials) were randomly sampled from the experimental field. Then, a composite bulk sample was produced by thoroughly mixing all the cores to measure SOC and its composition. Total SOC stock (Mg C ha^{-1}) in the 0–30 cm soil layer and its three component fractions [POC, MOC and charred organic carbon (COC)] were determined, at a minimum, at the start and end of each trial. Here, we would like to note that in most Australian ecosystems due to frequent perturbation by fire, COC is a critical component of total SOC (Schmidt et al., 1999; Jones et al., 2019). COC has a poly-aromatic chemical structure and is chemically recalcitrant to decomposition with a residence time ranging from centuries to millennia (Skjernstad et al., 1999; Baldock et al., 2013). Separating COC from total SOC enables more accurate quantification of POC and MOC and eliminating its potential confounding effects on POC and MOC dynamics. The three fractions were derived by physical fractionation, photo-oxidation and ^{13}C NMR spectroscopy (Skjernstad et al., 1999; Skjernstad et al., 2004). Briefly, soil samples were dispersed and then sieved into a coarse fraction (53 µm–2 mm) and a fine fraction (<53 µm). Total organic carbon (TOC) present in each fraction, respectively, was determined using the LECO combustion furnace method. COC content was determined for each fraction with photo-oxidation and ^{13}C NMR spectroscopy. Then, POC (i.e. TOC in the coarse fraction excluding COC) and MOC (i.e. TOC in the fine fraction excluding COC) were calculated as the TOC in the coarse and fine fractions excluding COC in that fraction, respectively. This SOC fractionation procedure has been successfully used to quantify SOC composition in Australia (Viscarra Rossel et al., 2019). The approach used to measure POC and MOC here align well with the framework proposed by Lavallee et al. (2020).

2.2. Carbon models driven by POC, MOC and COC

A parsimonious SOC model was designed to simulate the dynamics of POC and MOC (the M3 model, Fig. 1a). As COC is chemically resistant to decomposition (Skjernstad et al., 1999; Baldock et al., 2013) and was very stable at different time points of measurements at the same site, the model does not explicitly simulate COC but treats it as a constant estimated as the average of time-course measurements in each trial. The M3 model is written as:

$$\frac{dPOC}{dt} = I - k_{POC} \cdot POC, \quad (1)$$

$$\frac{dMOC}{dt} = e \cdot k_{POC} \cdot POC - k_{MOC} \cdot MOC \quad (2)$$

where I is the carbon input in $Mg\text{ C ha}^{-1}$, k_{POC} the decay rate of POC (yr^{-1}), e the transfer coefficient of decomposed POC that is recycled to MOC (unitless), k_{MOC} the decay rate of MOC (yr^{-1}).

There is evidence that a fraction of MOC is protected from decomposition because of its binding with minerals and/or other protection processes (Lavallee et al., 2020). To take into account this, another four-pool model (the M4 model, Fig. 1b) was developed to include a labile pool of MOC (MOC_l) which is readily available for decomposition. The remaining fraction of MOC is considered as a protected pool (MOC_p). The Langmuir isotherm (Ahrens et al., 2015) was used to simulate the transfer (i.e., adsorption/desorption processes) between MOC_l and MOC_p. In the M4 model, POC is simulated as in M3, but equation (2) is revised to:

$$\frac{dMOC_l}{dt} = e \cdot k_{POC} \cdot POC - k_{MOC_l} \cdot MOC_l - k_{ads} \cdot (q_{max} - MOC_p) \cdot MOC_l + k_{des} \cdot MOC_p, \quad (3)$$

and, the dynamics of MOC_p are simulated as:

$$\frac{dMOC_p}{dt} = k_{ads} \cdot (q_{max} - MOC_p) \cdot MOC_l - k_{des} \cdot MOC_p, \quad (4)$$

where k_{MOC_l} is the decay rate of MOC_l (yr^{-1}), q_{max} the maximum MOC sorption capacity of the soil ($Mg\text{ C ha}^{-1}$), k_{ads} the adsorption coefficient (yr^{-1}), and k_{des} the desorption coefficient (yr^{-1} , Table 1). At any time (i.e., year in this study), MOC is the sum of MOC_l and MOC_p:

$$MOC = MOC_l + MOC_p. \quad (5)$$

The two models (M3 and M4) do not explicitly consider the effect of environmental attributes. Rather, trial-specific parameter values were determined via optimization (see *Data assimilation* section). This simplification implicitly assumes that model parameters could vary across space and trials due to the variance of soil and climate conditions and management. The study sites cover most Australian agricultural

Table 1
Model parameters and their prior ranges used for model optimization.

Parameter	Description	Unit	Lower Limit	Upper Limit
k_{POC}	Decay rate of POC	yr^{-1}	0.1	1
e	Fraction of decomposed POC recycled to MOC	–	0.1	0.9
k_{MOC}	Decay rate of MOC in M3 model (MOC _l in the M4 model)	yr^{-1}	1×10^{-5}	0.1
f_{MOC}	Initial fraction of labile MOC fraction in total MOC (M4 model only)	–	0	1
q_{max}	Maximum adsorption capacity of MOC _l (M4 model only)	$Mg\text{ C ha}^{-1}$	0	200
k_{ads}	Adsorption coefficient of MOC _l (M4 model only)	yr^{-1}	0	0.2
k_{des}	Desorption coefficient of MOC _p (M4 model only)	yr^{-1}	0	0.2

areas (Fig. S1). With these data, the two models provide an opportunity to assess how optimized model parameters, which reflect the turnover behaviour of POC and MOC, are influenced by model structure and vary across the trials with the consideration of trial-specific management practices (e.g., crop-pasture rotation) and local environmental conditions.

2.3. Data assimilation

Using the measurements of SOC fractions in each trial, Bayes' theorem was used to optimize model parameters (i.e., k_{POC} , e and k_{MOC} for the M3 model, k_{POC} , e , k_{MOC_l} , k_{ads} , k_{des} and q_{max} for the M4 model) and initial conditions (Luo et al., 2011, 2017a). We ran the models at yearly time step to capture the observed temporal changes in POC and MOC. For each trial, the sum of the probability density of predictions (θ) was maximized to achieve the best agreement between model predictions and observations:

$$\theta = \sum_{j=1}^2 \sum_{i=1}^n \frac{1}{\sqrt{2 \cdot \pi \cdot \sigma_{j,i}^2}} \exp \left(-\frac{(x_{j,i} - \mu_{j,i})^2}{2 \cdot \sigma_{j,i}^2} \right), \quad (6)$$

where $\mu_{j,i}$ is the observed j th variable (i.e., POC or MOC) of i th observations, $\sigma_{j,i}$ is the standard deviation of j th variable of i th observations which was assigned to be 5% of $\mu_{j,i}$ as it was not reported in the dataset, $x_{j,i}$ is the corresponding model predictions, n is the sample size of observations in the trial. Model parameters were assumed to be distributed uniformly within their prior ranges (Table 1).

In the models, new carbon inputs were estimated as the sum of aboveground residue carbon retained and root carbon was estimated as 40% of total aboveground carbon (yield + residue) (Pausch and Kuzyakov, 2018). The initial fraction of POC and MOC in TOC was assigned according to measurements. For the M4 model, the initial fraction of labile MOC_l in total MOC (f_{MOC}) was optimized with other model parameters. Posterior probability distributions of parameters were obtained using the differential evolution adaptive metropolis (DREAM) algorithm by running three Markov Chain Monte Carlo (MCMC) chains (ter Braak and Vrugt, 2008; Vrugt and Ter Braak, 2011). Gelman–Rubin diagnostic index (G) was used to determine the convergence of MCMC simulations (Brooks and Gelman, 1998). If within-run variation within each MCMC chain is equal to the between-run variation among chains (i.e., $G = 1$), the simulations have converged. However, G cannot reach the exact value of 1. Here, we set a threshold of 1.01 for all parameters. That is, if G is less than 1.01 for all parameters, the MCMC simulations were considered to have converged. The MCMC was run using the runMCMC function in package BayesianTools in R version 4.1.2 (<https://www.r-project.org/>).

To explore the potential influence of using measured SOC fractions on model parameters as well as on model outputs, we also optimized the two models using only TOC. The two models were optimized using the same data assimilation approach as described above, but the initial fractions of POC, MOC and COC in TOC in both models were optimized with the other model parameters rather than assigned directly based on measurements. The optimized model parameters and performance of the two model configurations (i.e., optimization using TOC only vs using measured POC, MOC and COC fractions) on simulating POC, MOC and TOC were compared. Hereafter, data assimilation using measured fractions vs using TOC alone for the M3 model were referred as M3_{fraction} vs M3_{TOC}. For the M4 model, they were referred as M4_{fraction} vs M4_{TOC}. For each trial, we calculated parameter uncertainty quantified as the difference between 97.5% and 2.5% quantiles of the posterior distribution for each parameter, and compared this uncertainty between the two model configurations for the two models (i.e., M3_{fraction} vs M3_{TOC}, and M4_{fraction} vs M4_{TOC}). A paired *t*-test was conducted to test whether the uncertainty was significantly different ($P < 0.05$) across the trials.

Based on the posterior parameter matrix (each row includes one

ensemble of optimized parameters), a collinearity index γ in each trial was calculated to indicate parameter identifiability (Brun et al., 2001):

$$\gamma = \frac{1}{\sqrt{\min(\text{EV}[\hat{P}^T \hat{P}])}} \quad (7)$$

and,

$$\hat{P}_{ij} = \frac{P_{ij}}{\sqrt{\sum_j P_{ij}^2}}, \quad (8)$$

where \hat{P} is the matrix of posterior parameter ensembles, EV estimates the eigenvalue of the matrix. This collinearity index means that the fraction of $1 - 1/\gamma$ of a change in modelling results caused by a change in one parameter can be compensated by an appropriate change of other parameters. If $\gamma = 1$ (i.e., $1 - 1/\gamma = 0$), parameters are identifiable; if $\gamma = \infty$, parameters are linearly dependent and non-identifiable. Typically, $\gamma > 10$ is chosen to indicate that parameters are poorly identifiable (Brun et al., 2001). The collinearity index was calculated using the function `collin` in the package FME (Soetaert and Petzoldt, 2010) in R 4.1.2. In addition, we conducted pairwise correlation analysis to assess the covariance among parameters in each trial.

2.4. Environmental controls on model parameters

Multivariate linear regressions were conducted to evaluate the effects of environmental factors [which were also derived from Skjemstad and Spouner (2003) and include mean annual temperature and precipitation (MAT and MAP), agricultural management indicated by the fraction of pasture in the rotation system (fPasture), soil bulk density (BD), soil clay content, soil pH, soil SiO₂, Al₂O₃ and Fe₂O₃ content] on the mean of posterior distribution of model parameters under M3_{fraction} and M4_{fraction}, respectively. The variables were selected to determine those that better explained the optimized parameter values by backward-selection method based on adjusted determinant coefficient (R^2). Before fitting the model, all variables were standardized using *z-score*. Besides the multivariate linear model, a boosted regression tree (BRT) analysis was also conducted using the same set of environmental factors to account for interactions and nonlinear relationships between the variables (Elith et al., 2008). The BRT is a type of machine-learning algorithm that combines regression trees and boosting. It can identify the relative importance (RI, i.e., percentage influence or contribution) of individual explanatory variables compared to other variables (Elith et al., 2008). The BRT model was performed using the function `gbm.step` in the package `dismo` in R 4.1.2.

2.5. Quantification of uncertainty in SOC predictions

We sampled 200 parameter ensembles from the posterior parameter distribution to conduct simulations to explore the effects of modelling SOC fractions on SOC predictions. For both models (M3 and M4), using model parameters optimized using the two model configurations (M3_{fraction} vs M3_{TOC}, and M4_{fraction} vs M4_{TOC}) for each trial, respectively, the model was run for 100 years with carbon inputs being equal to the average of observed values during the trial. The vulnerability of SOC indicated by POC/(MOC + COC) (Viscarra Rossel et al., 2019) was calculated. The percentage uncertainty of simulated TOC and vulnerability at the end of the 100-year simulation in each trial were calculated as:

$$U = \frac{Q_{97.5} - Q_{2.5}}{Q_{50}} \times 100\%, \quad (9)$$

where Q_{2.5}, Q₅₀ and Q_{97.5} are the 2.5%, 50% (i.e., median) and 97.5% quantiles of the simulated TOC and vulnerability in the 200 simulations. Paired *t*-test was conducted to assess whether the simulated TOC and

vulnerability were significantly different ($P < 0.05$) between M_{fraction} and M_{TOC}.

3. Results

3.1. Model performance

Pooling together all data from the 159 trials, optimized M3 and M4 models driven by POC and MOC (i.e., M3_{fraction} and M4_{fraction}) explained 98% ($P < 0.001$) of the variance in observed TOC (Figs. 2a and 3a). In a trial at Brigalow as an illustrative example, it is clear that the optimized models well captured the temporal dynamics of observed TOC (Figs. 2b and 3b). In term of POC and MOC, the M3 model optimized using measured POC and MOC (i.e., M3_{fraction}) explained 89% and 95% of their variances, respectively (Fig. 2c,e), while the M4 model (i.e., M4_{fraction}) explained 89% and 97%, respectively (Fig. 3c,e). The temporal dynamics of POC and MOC in all trails were also well simulated by M3_{fraction} and M4_{fraction} as illustratively demonstrated by the results in a trial at Brigalow (Fig. 2d,f and 3d,f). When the models were optimized using TOC alone (M3_{TOC} and M4_{TOC}), both models could explain 98% of the variance of TOC (Figs. 2a and 3a), but neither could capture POC and MOC dynamics (Fig. 2c,e and 3c,e). Specifically, M3_{TOC} only explained 7% and 35% of the variance of POC and MOC, respectively (Fig. 2c,e), while M4_{TOC} explained 1% and 22%, respectively (Fig. 3c,e). The illustrative example at Brigalow also shows that simulated POC and MOC by M3_{TOC} and M4_{TOC} varied widely and could not capture the temporal dynamics of the two fractions (Fig. 2d,f and 3d,f).

3.2. Posterior parameter distributions and parameter identifiability

For the M3 model, uncertainties in k_{POC} and e were significantly reduced across the trials under M3_{fraction} compared with that under M3_{TOC} (Fig. 4a). For the M4 model, the uncertainties in five of the seven parameters (k_{POC} , e , k_{des} , q_{max} and f_{MOC}) were significantly reduced under M4_{fraction} compared with that under M4_{TOC}, but the uncertainties of other two parameters (k_{MOC} and k_{ads}) were significantly increased (Fig. 4a). In terms of the average of the posterior distribution of each parameter in each trial, its distribution across the trials was also significantly different between M3_{TOC} and M3_{fraction} for all three parameters (Fig. 4b). In general, model parameters varied widely across the trials irrespective of model structure and configuration approach. Under M3_{fraction}, averaging across the trials, median k_{POC} , e and k_{MOC} were estimated to be 0.46 yr^{-1} , 0.36 and 0.044 yr^{-1} , respectively. Under M4_{fraction}, averaging across the trials, median k_{POC} , e , k_{MOC} , k_{ads} , k_{des} , q_{max} , and f_{MOC} were estimated to be 0.46 yr^{-1} , 0.28 , 0.068 yr^{-1} , 0.0072 yr^{-1} , 0.10 yr^{-1} , 40 Mg C ha^{-1} and 0.72 , respectively. Fig. 4c shows an illustrative example of posterior distribution of model parameters in a trial at Brigalow. M3_{fraction} and M4_{fraction} reduced the uncertainties in parameters of M3 and M4 models, respectively (Fig. 4c).

Optimized model parameters under M3_{fraction} on average presented the lowest collinearity across the trials, followed by M3_{TOC}, M4_{TOC} and M4_{fraction} (Fig. 6). Especially, parameter collinearity did not show significant difference between M4_{TOC} and M4_{fraction} (Fig. 6). In terms of pairwise correlations between optimized model parameters, across the trials, the correlation of k_{POC} with e was much weaker under M3_{fraction} than under M3_{TOC} with an average correlation coefficient of 0.02 and 0.1, respectively (Fig. 5). However, the positive correlation between e and k_{MOC} became stronger under M3_{fraction}, with an average correlation coefficient of 0.83 and 0.39 under M3_{fraction} and M3_{TOC}, respectively. For other parameters under M3_{TOC} that were not required to be optimized under M3_{fraction}, both negative and positive correlations were common (Fig. 5). Particularly, in some trials, the correlation between e and f_{POC} was strong with correlation coefficients of greater than 0.5. For the M4 model, the correlation of k_{POC} with other parameters was weaker under M4_{fraction} than under M4_{TOC} (Fig. S2). However, M4_{fraction} did not consistently reduce the correlation between other variables compared

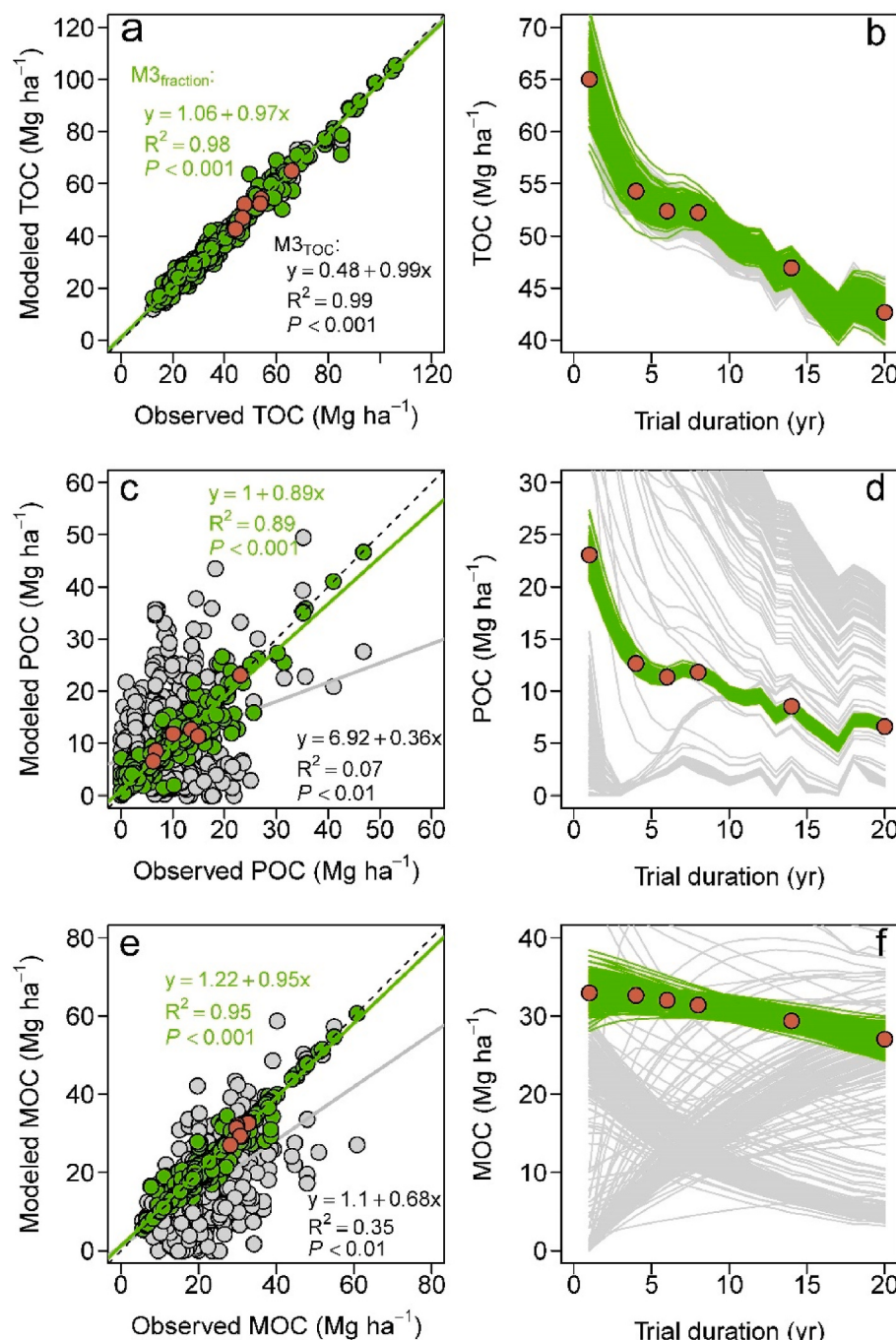


Fig. 2. Model performance of the three-pool model (M3). Left panels (a, c and e), the relationship between modelled and observed total soil carbon (TOC) and its fractions (i.e., POC and MOC) simulated by models constrained by all C fractions (M3_{fraction}, green circles) and TOC alone (M3_{TOC}, grey circles). Modelled values are the average of 200 simulations using 200 parameter ensembles sampled from posterior parameter distributions. Brown circles highlight the observed values in a trial as demonstrated in the right panels. The dashed lines show the 1:1 line. Right panels (b, d and f), a demonstrating example of modelled temporal carbon dynamics using 200 parameter ensembles constrained by carbon fractions (M3_{fraction}, green lines) and TOC alone (M3_{TOC}, grey lines). See Fig. 3 for the results of the four-pool model (M4). (For interpretation of the references to colour in this figure legend, the reader is referred to the Web version of this article.)

with M4_{TOC} (Fig. S2).

3.3. Environmental controls over optimized model parameters

Focusing on the median of posterior parameter values optimized under M3_{fraction} and M4_{fraction}, multivariate linear regression suggested that 37% of the variance of k_{POC} across the 159 trials could be explained by the selected variables (Fig. 7a). Soil Fe₂O₃ and SiO₂ contents were the most important variables positively affecting k_{POC} under both M3_{fraction} and M4_{fraction} (Fig. 7a). For e and k_{des} under M4_{fraction}, 38% and 49% of their variances, respectively, could be also explained. Particularly, e showed the strongest negative association with soil Fe₂O₃ and SiO₂ contents, and k_{des} showed positive correlation with clay and SiO₂ contents. For all other parameters regardless of model configuration

approach, the linear regression could only explain <30% of their variances (Fig. 7a). Compared to the multivariate linear regression, the BRT model could explain more variances of the optimized parameter values (Fig. 7b). For example, the selected variables could explain 77% of the variance of k_{POC} , while MAT (which alone contributed 24% to the explained variance) and BD (21%) were the two most important variables under both M3_{fraction} and M4_{fraction} (Fig. 7b). For e and k_{des} under M4_{fraction}, the selected variables could explain more than 60% of their variances, while MAP was the most important for both parameters (Fig. 7b).

3.4. Prediction uncertainties

Predictions of both TOC and its vulnerability, using M3_{fraction} and

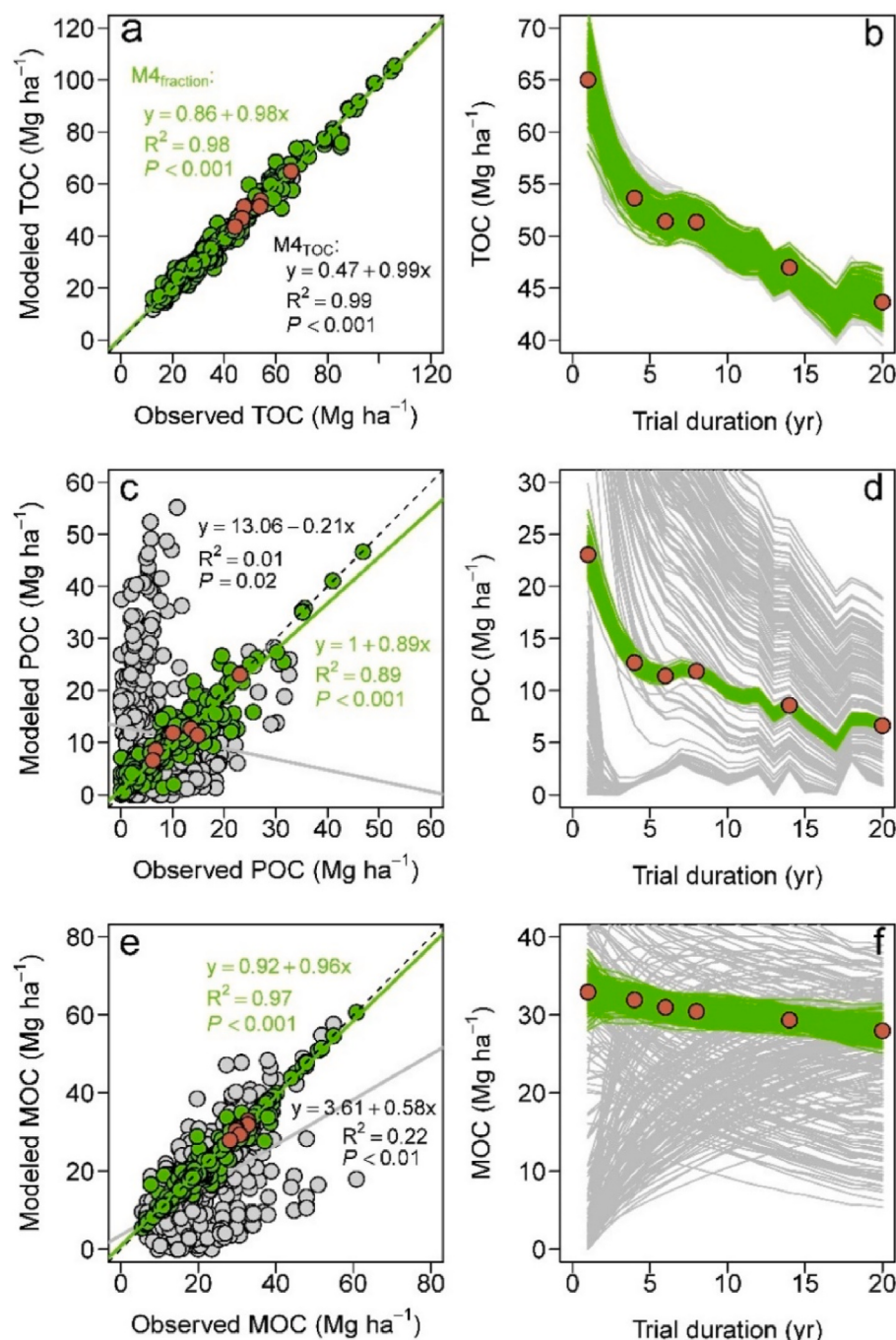


Fig. 3. Model performance of the four-pool model (M4). Left panels (a, c and e), the relationship between modelled and observed total soil carbon (TOC) and its fractions (i.e., POC and MOC) simulated by models constrained by all C fractions (M_{fraction}, green circles) and TOC alone (M_{TOC}, grey circles). Modelled values are average of simulations using 1000 parameter ensembles sampled from posterior parameter distributions. Brown circles highlight the observed values in a trial as demonstrated in the right panels. Right panels (b, d and f), a demonstrating example of modelled temporal C dynamics using 200 parameter ensembles (lines). The dashed lines show the 1:1 line. (For interpretation of the references to colour in this figure legend, the reader is referred to the Web version of this article.)

M4_{fraction} over the 100-year simulations, were less uncertain compared to M3_{TOC} and M4_{TOC}, respectively (Fig. 8). In a trial at Brigalow, for example, TOC ranged from 21 to 37 Mg ha⁻¹ at the end of the 100-year simulation under M3_{fraction}, while it ranged from 17 to 81 Mg ha⁻¹ under M3_{TOC} (Fig. 9a). The potential vulnerability of TOC calculated with M3_{fraction} and M4_{fraction} was also less uncertain than that of M3_{TOC} and M4_{TOC}, respectively (Fig. 9b,d). Across the 159 trials, overall, M3_{fraction} predicted significantly lower median TOC (i.e., 50% quantiles of the 200 simulations at each trial) than M3_{TOC}, while M4_{fraction} and M4_{TOC} predicted comparable median TOC (Fig. 8a). However, the uncertainty under both M3_{fraction} and M4_{fraction} was significantly smaller than that under M3_{TOC} and M4_{TOC} (Fig. 8b). Both M3_{fraction} and M4_{fraction} predicted significantly higher but much less uncertainty in vulnerability than M3_{TOC} and M4_{TOC}, respectively (Fig. 8d). It is also noteworthy that,

among the two model structures and two configurations, M3_{fraction} consistently predicted the lowest uncertainty in both TOC and its vulnerability (Fig. 8).

4. Discussion

4.1. POC and MOC turnover behaviours

M3_{fraction} and M4_{fraction} models predicted the same decay rate of POC with an average of 0.46 yr⁻¹ (i.e., ~2 years in terms of residence time) ranging from 1 to 10 years across the 159 trials. This estimation of ~2 years of POC residence time is in the same order of the estimate of ~7 years by other authors (Skjemstad et al., 2004; Baldock et al., 2013). For the decay rate of MOC, M3_{fraction} predicted an average value of 0.044

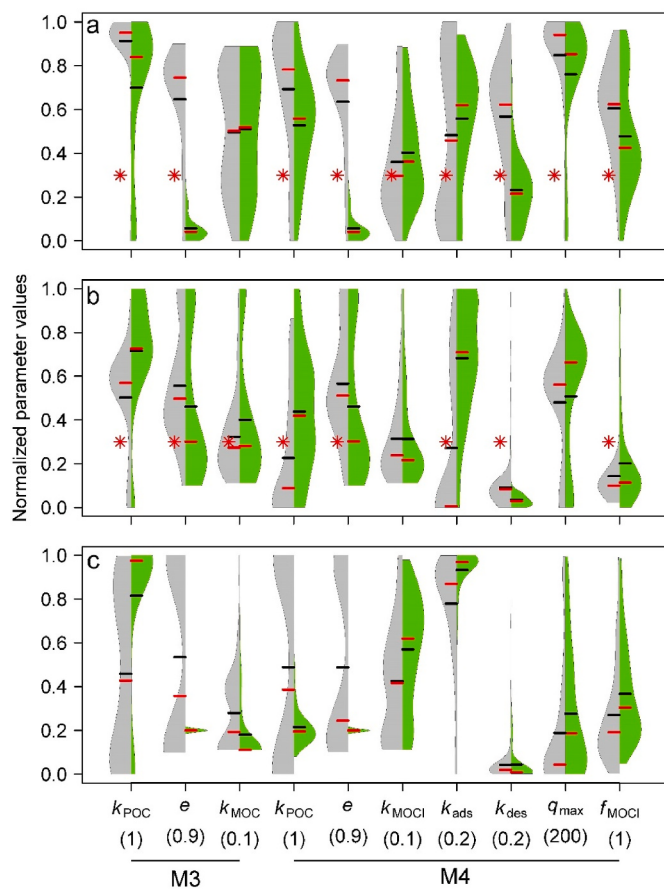


Fig. 4. Parameter uncertainties and posterior distributions in the M3 and M4 models. **a**, the distribution of parameter uncertainty (i.e., the difference between 97.5% and 2.5% quantiles of the posterior distribution of model parameters) across the 159 trials using measured carbon fractions (green colour, M3_{fraction} and M4_{fraction}) and TOC alone (grey colour, M3_{TOC} and M4_{TOC}). **b**, the distribution of the median of posterior model parameter distribution across the 159 trials. **c**, an example demonstrating the posterior distribution of model parameters in a trial at Brigalow. *, significantly different at the level of $P < 0.05$. Black and red ticks show the mean and median, respectively. All values are normalized to the range from 0 to 1 by dividing the values shown in the corresponding parentheses, which are the upper limits of the prior distribution of the parameter shown in Table 1. (For interpretation of the references to colour in this figure legend, the reader is referred to the Web version of this article.)

yr^{-1} (which is equivalent to a residence time of 22 years), which is also similar to that predicted by Skjemstad et al. (2004) and Baldock et al. (2013). It should be noted that the decay rates of POC and MOC were derived from in situ measurements of POC and total MOC fractions. Thus, the maximum potential decay rates of the two pools at optimal environmental conditions could be faster. Indeed, our analyses indicated that k_{POC} was regulated by a number of environmental factors with strong linear association with soil SiO₂ and Fe₂O₃ contents which reflect soil mineralogy (Fig. 7a). However, when taking into account nonlinear relationships and interactions, MAT and BD were identified to be the two most important individual variables (Fig. 7b). Similarly, MOC dynamics were also influenced by various environmental factors but more difficult to be explained. Particularly, MAP consistently showed the strongest effect on k_{MOC} (k_{MOCl}), k_{des} , q_{max} . These results suggest that various direct and indirect but distinct processes are involved in POC and MOC dynamics (Luo et al., 2020; Mao et al., 2022).

M₄fraction simulations provided additional insights into MOC dynamics, and supported the knowledge that a large fraction of MOC is

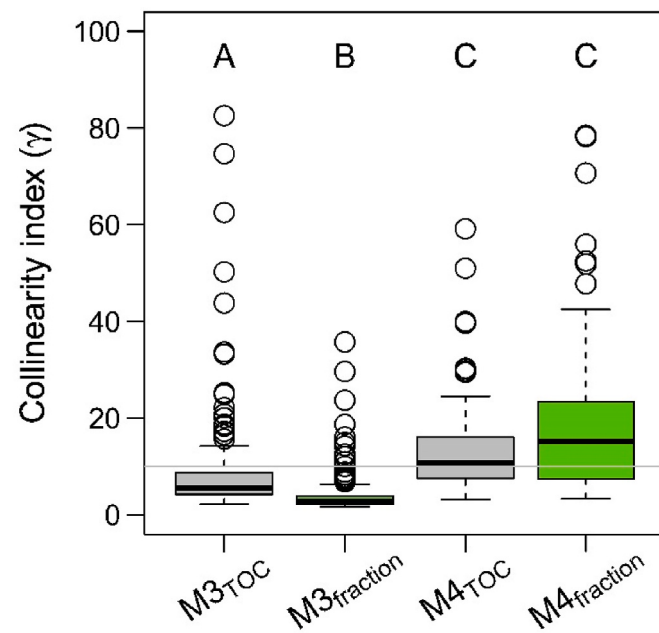


Fig. 6. Parameter collinearity (γ) in two models and under two configurations. Boxplots show the median and interquartile range with whiskers extending to 1.5 times of the interquartile range. Grey horizontal line shows the threshold value of poor identifiability, i.e., $\gamma = 10$. Different capital letters indicate significant difference at $P < 0.05$. Some extreme large values of γ are not presented.

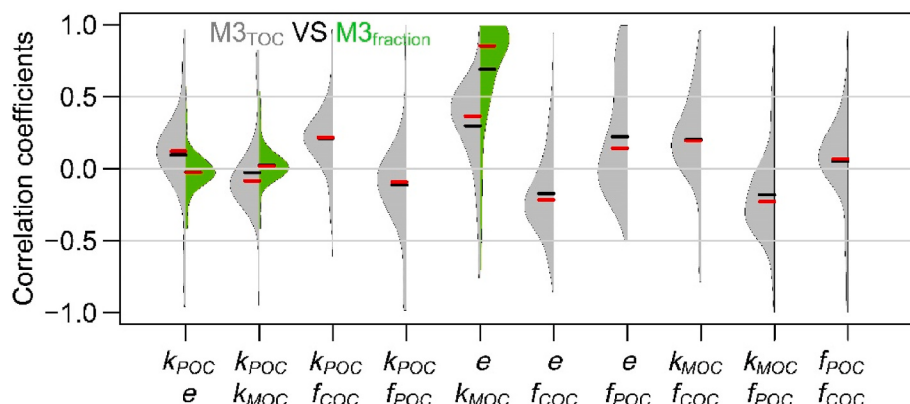


Fig. 5. The distribution of pairwise correlation coefficients between model parameters within the 200 posterior parameter ensembles in the M3 model across the 159 trials. Black and red ticks show the mean and median, respectively. Some parameters are not needed to be optimized under M3_{fraction}, and thus the distributions of their correlation coefficients with other parameters are unavailable. (For interpretation of the references to colour in this figure legend, the reader is referred to the Web version of this article.)

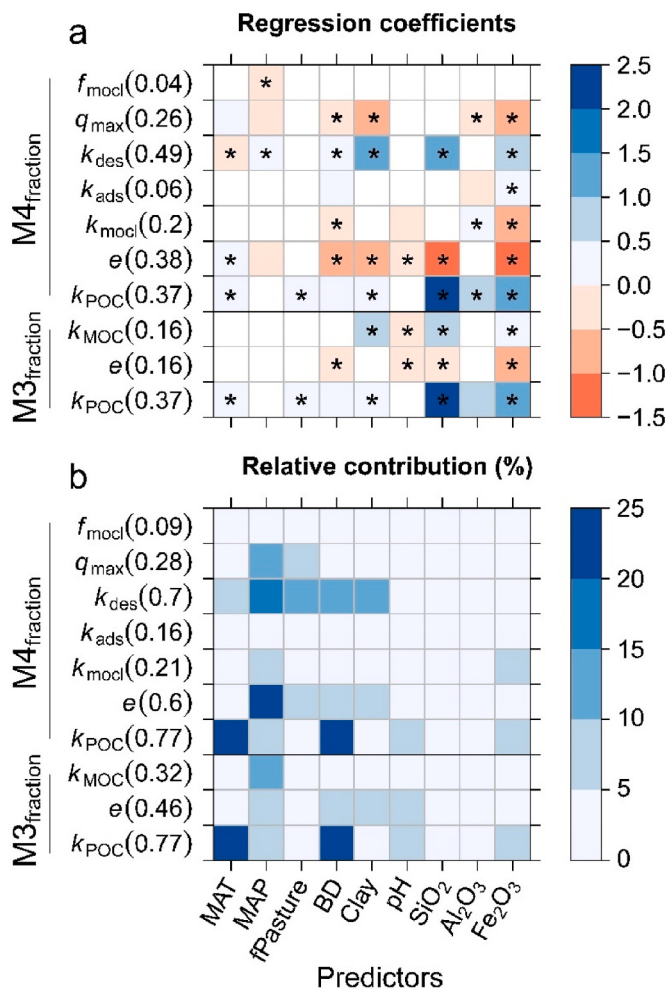


Fig. 7. Environmental controls over model parameters optimized under M3fraction and M4fraction across the 159 trials. **a**, regression confidences for multivariate linear regression. * indicates that the regression coefficient is significant at $P < 0.05$. **b**, relative importance identified by boosted regression trees. Numbers in the parentheses show the coefficient of determination (i.e., R^2) of the model for the corresponding parameter. Blank pixels indicate that the predictor is not included in the model.

inaccessible to microbial decomposition due to physical protection such as organo-mineral binding and occlusion within soil aggregates (Dungait et al., 2012; Luo et al., 2017b; Lavallee et al., 2020). Indeed, M4fraction predicted that on average 28% of MOC ($f_{MOC} = 0.72$, i.e., 28% of MOC is MOC_p) is unavailable for decomposition, which can also be verified by long-term field observations focusing on bare soils. A series of studies have found that, after decades of zero soil carbon inputs (i.e., bare soil), soil carbon loss is stable and small following the larger carbon loss at the start of the experiment, but can be subsequently stimulated by tillage (Balesdent et al., 2000; Plante and McGill, 2002). Such physical soil disturbances (e.g., tillage) destruct soil matrix (e.g., soil aggregates and organo-mineral associations) therefore exposing protected SOC to microbial decomposition. Direct empirical measurements on the underlying protection processes and how these processes respond to management and environmental changes will be essential for MOC predictions under frequent disturbance that influences MOC protection processes.

The M4 modelling results supported the idea that MOC saturates due to finite amount of mineral specific surface area onto which MOC can stabilize (Six et al., 2002; Stewart et al., 2007), reflected by the parameter q_{max} which defines the maximum adsorption capacity. If a soil reaches its maximum protection capacity, no more MOC can be

protected (i.e., MOC saturation) and overall SOC stability will decrease (Feng et al., 2014). Our estimation of this capacity on average is ~40 Mg C ha⁻¹ (Fig. 4b), which is in line with the observed maximum MOC stock of 20–45 Mg C ha⁻¹ in Europe (Cotrufo et al., 2019). However, it should be noted that the estimated capacity by the model varies widely across the trials ranging from <3 to >40 Mg C ha⁻¹. This result may be due to the diverse climate and soil conditions as well as agricultural management (Fig. 7). Indeed, some studies have demonstrated that both land management and climatic condition influence SOC saturation (Angers et al., 2011; Wiesmeier et al., 2018). After reaching such saturation, if more MOC is produced due to any reasons (e.g., microbial debris replenishment), these additional MOC will be subject to rapid decomposition (e.g., at the rate of ~0.069 yr⁻¹ estimated by M4fraction) rather than accrual. As both POC and MOC are potentially more vulnerable to decomposition (i.e., fast decay rates), MOC protection capacity of soil would be the bottleneck of long-term SOC sequestration in the MOC pool, and effective management of the two pools will be essential.

4.2. Insights into pool-based SOC modelling

Our results demonstrated that POC, MOC and COC measurements can promote accurate simulation of the dynamics of individual pools in pool-based models. Using measured fractions have advantages overcoming several challenges in conceptualizing, initializing and/or parameterizing SOC pools (Skjemstad et al., 2004; Zimmermann et al., 2007; Lee and Viscarra Rossel, 2020; Abramoff et al., 2022; Dangal et al., 2022). For example, verifying pools with slow decay rates in most pool-based models is usually empirically impossible due to that most experiments do not last long enough to collect required data. This would result in great uncertainties in predictions of the slow pool which usually accounts for the majority of total SOC pool (Balesdent et al., 2018). COC is clearly defined as biologically recalcitrant chemical fractions (Baldock et al., 2013), facilitating initialization of the slow pool. Additionally, conventional pool-based simulations commonly depend on model-fitting techniques to derive the sizes of most pools rather than using measured pools to directly test model performance of simulating individual pools. Our results (M3TOC vs M3fraction and M4TOC vs M4fraction) demonstrate that this fitting cannot capture real dynamics of POC and MOC. This mismatch is the direct reason underlying the larger uncertainties in terms of both TOC and its vulnerability in M3TOC and M4TOC predictions compared with M3fraction and M4fraction (Fig. 8). Pool-based models are a key tool to project SOC dynamics. Temporal measurements of functionally distinct SOC fractions like POC, MOC and COC can reduce uncertainties in the estimation of decay rates of pools as well as the transfer between pools (Fig. 4). Models explicitly simulating functionally distinct SOC pools with explicit consideration of stabilization and destabilization processes underpinning their dynamics are particularly important under global change as global change factors (e.g., warming, land use transition and changed drying-wetting cycle) can modify the processes involved in the dynamics of different pools (Luo et al., 2020; Lugato et al., 2021).

Although the two models used in this study are simple, the relevant results regarding the collinearity among and identifiability of model parameters and uncertainties induced by such identifiability may be general for pool-based models. First, it is reasonable to expect that if a simple model has the identifiability issue, more complex models may suffer from the issue more seriously. Our results indeed provide direct evidence that parameters in the four-pool model regardless of M4fraction and M4TOC are less identifiable compared with in the three-pool model (Fig. 7). Shi et al. (2018) also demonstrated that complex carbon models amplified the uncertainties predicted soil carbon dynamics in response to climate change. Although increasing model complexity may improve realism (e.g., reflecting physical protection process of MOC in this study), it is vital to consider parameter identifiability for assessing prediction accuracy (Luo et al., 2017a; Marschmann et al., 2019).

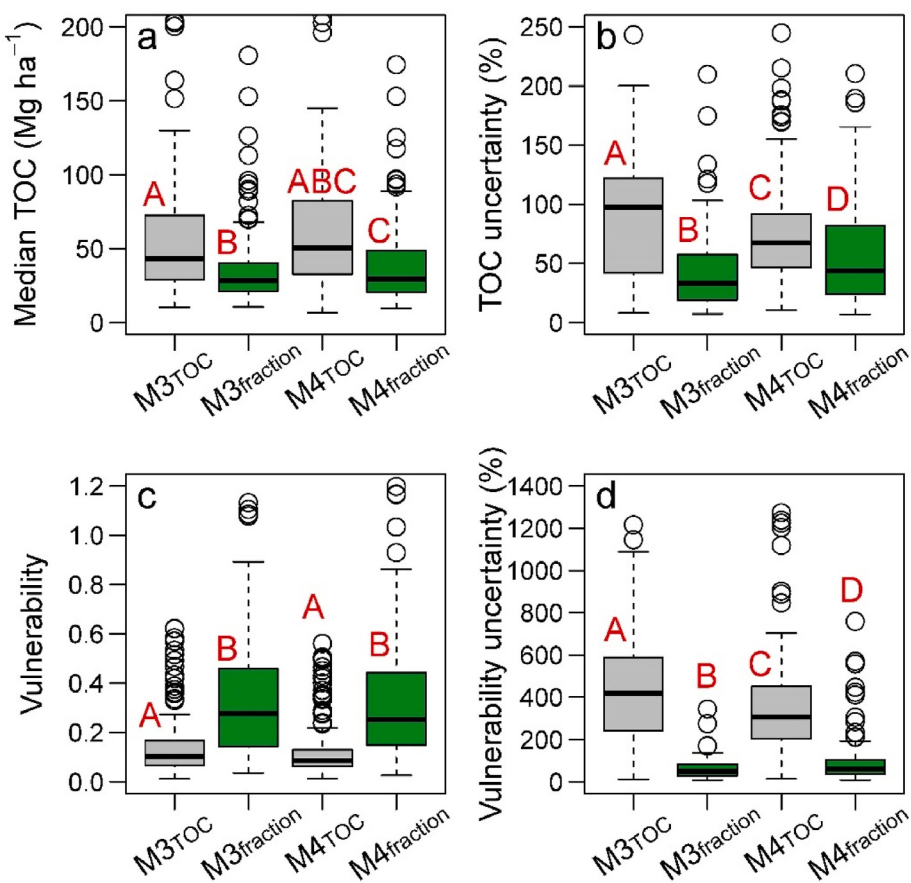


Fig. 8. Comparison of simulated soil organic carbon stock and its vulnerability across the 159 trials. Vulnerability is estimated as the ratio of POC to the sum of MOC and COC. Boxplots show the median and interquartile range with whiskers extending to 1.5 times of the interquartile range. Different capital letters indicate significant difference at $p < 0.05$.

Second, observational data aligning with model requirement is usually limited, particularly for complex models, hindering empirical model initialization and parameterization. It is easy to increase model complexity by including more pools or explicit processes. Our results demonstrate that increase of complexity (M3 results vs M4 results) does not improve model performance, if observed data does not increase correspondingly (Fig. 2 vs Fig. 3). This result is line with a modelling study using 16 different models of SOC cycle with different model complexity (Famiglietti et al., 2021). However, it should be highlighted that using POC, MOC and COC for model optimization significantly reduced uncertainties in predictions of SOC dynamics by both M3 and M4 (Fig. 8). To determine model complexity, we should consider the trade-off between data demand (which includes not only data amount but also the type of data) by models and data supply by observations (Luo et al., 2009).

4.3. Limitations and uncertainties

The models used in this study have some limitations. First, it relaxes the deterministic response of model parameters to environmental scalars, such as soil temperature and moisture response functions formulated in most models. The fitted parameter values reflect the integrated effects of environmental variables. A fundamental reason to do so is that functions modifying model parameters may not precisely capture their responses to climate or soil attributes. Indeed, our assessment of the environmental controls over the optimized model parameters demonstrated that the turnover of MOC and POC were controlled by distinct climate and soil properties with involvement of non-linear relationships (Fig. 7). Second, the model structure of both M3 and M4 is relatively

simple and does not consider microbial processes and detailed stabilization/destabilization processes. Over the course of the last decade, as the scientific community probed deeper into the complexities of SOC stabilization and destabilization mechanisms (Schmidt et al., 2011; Lehmann and Kleber, 2015), more explicit modelling frameworks and models have been developed such as MIMICS (Wieder et al., 2014), MEMS (Cotrufo et al., 2013; Robertson et al., 2019) and COMISSION (Ahrens et al., 2015). These models mechanistically simulate the formation, decomposition, stabilization and destabilization processes of SOC as the combined, integrated consequences of the quality of SOC inputs (e.g., plant litter), microbial activity and functioning, and soil matrix. Emerging new framework considers SOC cycling as a stochastic process governed by the proximity between microbial decomposers and organic substrates depending on their flow in the soil matrix (Waring et al., 2020). However, our data does not allow us to specifically drive those models as other more specific data, particularly those that represent microbial processes, are required to initialize and/or parameterize those models.

4.4. Conclusions

The parsimonious models that we present, driven by POC, MOC and COC, can well predict total SOC dynamics as well as its POC and MOC components if model parameters can be calibrated to capture observed MOC and POC. Compared with models constrained by total SOC alone, uncertainty in most model parameters as well as in model predictions has been significantly reduced. In addition, we found that vulnerability of SOC [indicated by $\text{POC}/(\text{MOC} + \text{COC})$] predicted by the two models with different complexity (M3 vs M4) and two configuration strategies

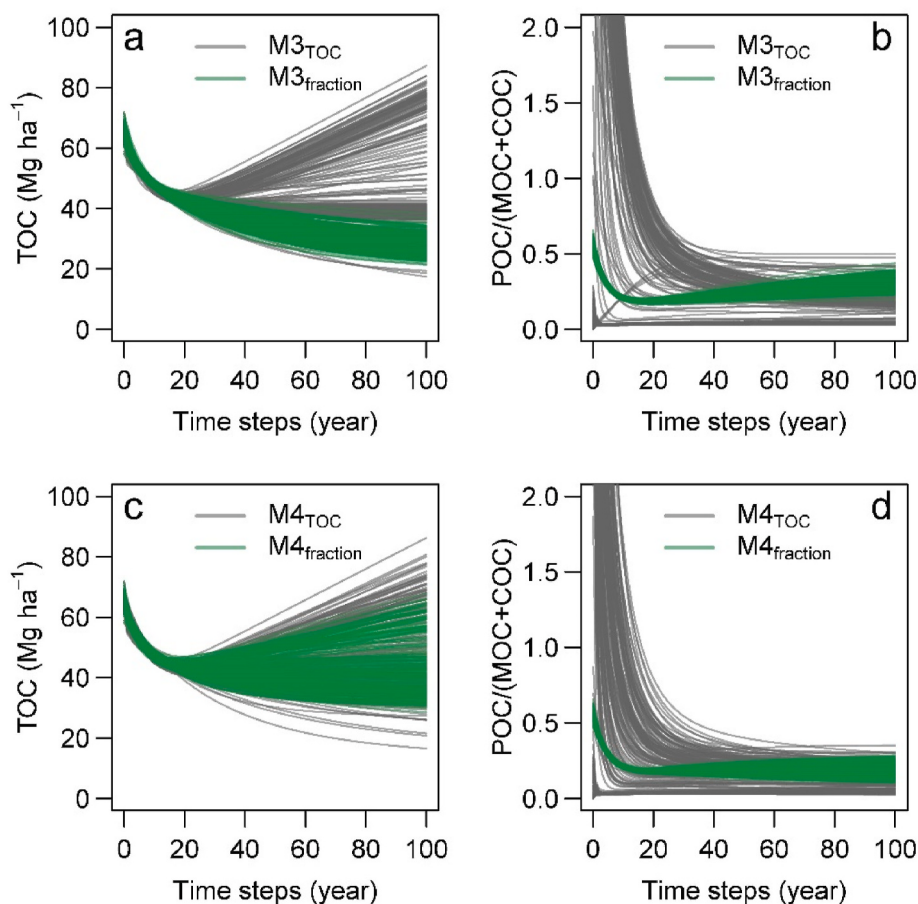


Fig. 9. An illustrative example of simulated evolution of total organic carbon (TOC) dynamics. (a) and (b) show the evolution of TOC and its vulnerability during a 100-year simulation in a trial at Brigalow, respectively. Vulnerability is estimated as the ratio of POC to the sum of MOC and COC.

were markedly different. This has significant consequences on the prediction of the fate of SOC under global change if model complexity and parameterization is not bounded with available observational data in terms of both data amount and type (e.g., POC, MOC and COC). The results also shed new lights on controls over turnover behaviors of POC and MOC, highlighting the requirement to explicitly quantify potential non-linear relationships of POC and MOC dynamics with climate and soil properties. Without quantitative information of MOC on its stabilization and destabilization processes, its overall decomposition and interactions with soil matrix and minerals are difficult to be predicted by measuring MOC alone. We need novel approaches to further explicitly separate MOC into labile and protected fractions, as well as to explore how the two fractions keep balance in the soil matrix. We suggest that using temporal measurements of POC and MOC to constrain SOC models could reduce uncertainties in both model parameters and predictions. However, model complexity should be carefully determined based on data availability taking into account parameter identifiability. The next step would be to explicitly quantify how carbon exchanges between POC and MOC vary with climate and soil properties, enabling their mathematical representation in SOC models. Overall, our results demonstrate that measured functional pools reduce uncertainties in model parameterization and initialization, promoting more informative and reliable prediction of SOC dynamics.

Declaration of competing interest

The authors declare the following financial interests/personal relationships which may be considered as potential competing interests: Zhongkui Luo reports financial support was provided by Ministry of

Science and Technology of the People's Republic of China.

Acknowledgements

We thank Francesca Cotrufo for helpful comments on an early version of this manuscript. Funding: this work was supported by the National Key Research & Development Program of Ministry of Science and Technology of China (grant no. 2021YFE0114500), the National Natural Science Foundation of China (grant no. 32171639, 41930754), and Fundamental Research Funds for the Central Universities (226-2022-00084).

Appendix A. Supplementary data

Supplementary data to this article can be found online at <https://doi.org/10.1016/j.soilbio.2022.108780>.

References

- Abramoff, R.Z., Guenet, B., Zhang, H., Georgiou, K., Xu, X., Viscarra Rossel, R.A., Yuan, W., Ciais, P., 2022. Improved global-scale predictions of soil carbon stocks with Millennial Version 2. *Soil Biology and Biochemistry* 164, 108466.
- Ahrens, B., Braakhekke, M.C., Guggenberger, G., Schrumpf, M., Reichstein, M., 2015. Contribution of sorption, DOC transport and microbial interactions to the 14C age of a soil organic carbon profile: insights from a calibrated process model. *Soil Biology and Biochemistry* 88, 390–402.
- Andrén, O., Kätterer, T., 1997. ICBM: the introductory carbon balance model for exploration of soil carbon balances. *Ecological Applications* 7, 1226–1236.
- Angers, D.A., Arrouays, D., Saby, N.P.A., Walter, C., 2011. Estimating and mapping the carbon saturation deficit of French agricultural topsoils. *Soil Use & Management* 27, 448–452.

- Baldock, J.A., Sanderman, J., Macdonald, L.M., Puccini, A., Hawke, B., Szarvas, S., McGowan, J., 2013. Quantifying the allocation of soil organic carbon to biologically significant fractions. *Soil Research* 51, 561–576.
- Balesdent, J., Basile-Doelsch, I., Chadoeuf, J., Cornu, S., Derrien, D., Fekiacova, Z., Hatté, C., 2018. Atmosphere–soil carbon transfer as a function of soil depth. *Nature* 559, 599–602.
- Balesdent, J., Chenet, C., Balabane, M., 2000. Relationship of soil organic matter dynamics to physical protection and tillage. *Soil and Tillage Research* 53, 215–230.
- Brooks, S.P., Gelman, A., 1998. General methods for monitoring convergence of iterative simulations. *Journal of Computational & Graphical Statistics* 7, 434–455.
- Brun, R., Reichert, P., Künsch, H.R., 2001. Practical identifiability analysis of large environmental simulation models. *Water Resources Research* 37, 1015–1030.
- Cotrufo, M.F., Ranalli, M.G., Haddix, M.L., Six, J., Lugato, E., 2019. Soil carbon storage informed by particulate and mineral-associated organic matter. *Nature Geoscience* 12, 989–994.
- Cotrufo, M.F., Wallenstein, M.D., Boot, C.M., Denef, K., Paul, E., 2013. The Microbial Efficiency-Matrix Stabilization (MEMS) framework integrates plant litter decomposition with soil organic matter stabilization: do labile plant inputs form stable soil organic matter? *Global Change Biology* 19, 988–995.
- Dangal, S.R.S., Schwalm, C., Cavigelli, M.A., Gollany, H.T., Jin, V.L., Sanderman, J., 2022. Improving soil carbon estimates by linking conceptual pools against measurable carbon fractions in the DAYCENT model version 4.5. *Journal of Advances in Modeling Earth Systems* 14 e2021MS002622.
- Dungait, J.A.J., Hopkins, D.W., Gregory, A.S., Whitmore, A.P., 2012. Soil organic matter turnover is governed by accessibility not recalcitrance. *Global Change Biology* 18, 1781–1796.
- Elith, J., Leathwick, J.R., Hastie, T., 2008. A working guide to boosted regression trees. *Journal of Animal Ecology* 77, 802–813.
- Famiglietti, C.A., Smallman, T.L., Levine, P.A., Flack-Prain, S., Quetin, G.R., Meyer, V., Parazoo, N.C., Stett, S.G., Yang, Y., Bonal, D., Bloom, A.A., Williams, M., Konings, A.G., 2021. Optimal model complexity for terrestrial carbon cycle prediction. *Biogeosciences* 18, 2727–2754.
- Feng, W., Plante, A.F., Aufdenkampe, A.K., Six, J., 2014. Soil organic matter stability in organo-mineral complexes as a function of increasing C loading. *Soil Biology and Biochemistry* 69, 398–405.
- Jenkinson, D.S., Rayner, J.H., 1977. Turnover of soil organic-matter in some of Rothamsted classical experiments. *Soil Science* 123, 298–305.
- Jones, M.W., Santín, C., van der Werf, G.R., Doerr, S.H., 2019. Global fire emissions buffered by the production of pyrogenic carbon. *Nature Geoscience* 12, 742–747.
- Lal, R., 2004. Soil carbon sequestration impacts on global climate change and food security. *Science* 304, 1623–1627.
- Lal, R., 2016. Soil health and carbon management. *Food and Energy Security* 5, 212–222.
- Lavallee, J.M., Soong, J.L., Cotrufo, M.F., 2020. Conceptualizing soil organic matter into particulate and mineral-associated forms to address global change in the 21st century. *Global Change Biology* 26, 261–273.
- Lee, J., Viscarra Rossel, R.A., 2020. Soil carbon simulation confounded by different pool initialisation. *Nutrient Cycling in Agroecosystems* 116, 245–255.
- Lehmann, J., Kleber, M., 2015. The contentious nature of soil organic matter. *Nature* 528, 60–68.
- Lugato, E., Lavallee, J.M., Haddix, M.L., Panagos, P., Cotrufo, M.F., 2021. Different climate sensitivity of particulate and mineral-associated soil organic matter. *Nature Geoscience* 14, 295–300.
- Luo, Y., Ahlström, A., Allison, S.D., Batjes, N.H., Brovkin, V., Carvalhais, N., Chappell, A., Ciais, P., Davidson, E.A., Finzi, A., Georgiou, K., Guenet, B., Hararuk, O., Harden, J. W., He, Y., Hopkins, F., Jiang, L., Koven, C., Jackson, R.B., Jones, C.D., Lara, M.J., Liang, J., McGuire, A.D., Parton, W., Peng, C., Randerson, J.T., Salazar, A., Sierra, C. A., Smith, M.J., Tian, H., Todd-Brown, K.E.O., Torn, M., van Groenigen, K.J., Wang, Y.P., West, T.O., Wei, Y., Wieder, W.R., Xia, J., Xu, X., Xu, X., Zhou, T., 2016. Toward more realistic projections of soil carbon dynamics by Earth system models. *Global Biogeochemical Cycles* 30, 40–56.
- Luo, Y., Ogle, K., Tucker, C., Fei, S., Gao, C., LaDau, S., Clark, J.S., Schimel, D.S., 2011. Ecological forecasting and data assimilation in a data-rich era. *Ecological Applications* 21, 1429–1442.
- Luo, Y., Weng, E., Wu, X., Gao, C., Zhou, X., Zhang, L., 2009. Parameter identifiability, constraint, and equifinality in data assimilation with ecosystem models. *Ecological Applications* 19, 571–574.
- Luo, Z., Viscarra Rossel, R.A., Shi, Z., 2020. Distinct controls over the temporal dynamics of soil carbon fractions after land use change. *Global Change Biology* 26, 4614–4625.
- Luo, Z., Wang, E., Sun, O.J., 2017a. Uncertain future soil carbon dynamics under global change predicted by models constrained by total carbon measurements. *Ecological Applications* 27, 1001–1009.
- Luo, Z., Baldock, J., Wang, E., 2017b. Modelling the dynamic physical protection of soil organic carbon: insights into carbon predictions and explanation of the priming effect. *Global Change Biology* 23, 5273–5283.
- Mao, X., Zheng, J., Yu, W., Guo, X., Xu, K., Zhao, R., Xiao, L., Wang, M., Jiang, Y., Zhang, S., Luo, L., Chang, J., Shi, Z., Luo, Z., 2022. Climate-induced shifts in composition and protection regulate temperature sensitivity of carbon decomposition through soil profile. *Soil Biology and Biochemistry*, 108743.
- Marschmann, G.L., Pagel, H., Kügler, P., Streck, T., 2019. Equifinality, sloppiness, and emergent structures of mechanistic soil biogeochemical models. *Environmental Modelling & Software* 122, 104518.
- Parton, W.J., Stewart, J.W., Cole, C.V., 1988. Dynamics of C, N, P and S in grassland soils: a model. *Biogeochemistry* 5, 109–131.
- Pausch, J., Kuzyakov, Y., 2018. Carbon input by roots into the soil: quantification of rhizodeposition from root to ecosystem scale. *Global Change Biology* 24, 1–12.
- Paustian, K., Lehmann, J., Ogle, S., Reay, D., Robertson, G.P., Smith, P., 2016. Climate-smart soils. *Nature* 532, 49–57.
- Plante, A.F., McGill, W.B., 2002. Soil aggregate dynamics and the retention of organic matter in laboratory-incubated soil with differing simulated tillage frequencies. *Soil and Tillage Research* 66, 79–92.
- Robertson, A.D., Paustian, K., Ogle, S., Wallenstein, M.D., Lugato, E., Cotrufo, M.F., 2019. Unifying soil organic matter formation and persistence frameworks: the MEMS model. *Biogeosciences* 16, 1225–1248.
- Schmidt, M.W.I., Skjemstad, J.O., Gehrt, E., Kögel-Knabner, I., 1999. Charred organic carbon in German chernozemic soils. *European Journal of Soil Science* 50, 351–365.
- Schmidt, M.W.I., Torn, M.S., Abiven, S., Dittmar, T., Guggenberger, G., Janssens, I.A., Kleber, M., Kögel-Knabner, I., Lehmann, J., Manning, D.A.C., Nannipieri, P., Rasse, D.P., Weiner, S., Trumbore, S.E., 2011. Persistence of soil organic matter as an ecosystem property. *Nature* 478, 49–56.
- Shi, Z., Crowell, S., Luo, Y., Moore, B., 2018. Model structures amplify uncertainty in predicted soil carbon responses to climate change. *Nature Communications* 9, 2171.
- Six, J., Conant, R.T., Paul, E.A., Paustian, K., 2002. Stabilization mechanisms of soil organic matter: implications for C-saturation of soils. *Plant and Soil* 241, 155–176.
- Skjemstad, J., Spounger, L.R., 2003. Integrated soils modelling for the national carbon accounting system (estimating changes in soil carbon resulting from changes in land use). Australian Greenhouse Office. Retrieved from. http://www.fullcam.com/FullC_AMServer/Help/reps/ (TR 36 Soils Modelling for NCAS).
- Skjemstad, J.O., Spounger, L.R., Cowie, B., Swift, R.S., 2004. Calibration of the Rothamsted organic carbon turnover model (RothC ver. 26.3), using measurable soil organic carbon pools. *Soil Research* 42, 79–88.
- Skjemstad, J.O., Taylor, J.A., Smernik, R.J., 1999. Estimation of charcoal (char) in soils. *Communications in Soil Science and Plant Analysis* 30, 2283–2298.
- Smith, J.U., Smith, P., Monaghan, R., MacDonald, A.J., 2002. When is a measured soil organic matter fraction equivalent to a model pool? *European Journal of Soil Science* 53, 405–416.
- Soetaert, K., Petzoldt, T., 2010. Inverse modelling, sensitivity and Monte Carlo analysis in R using package FME. *Journal of Statistical Software* 33, 1–28.
- Stewart, C.E., Paustian, K., Conant, R.T., Plante, A.F., Six, J., 2007. Soil carbon saturation: concept, evidence and evaluation. *Biogeochemistry* 86, 19–31.
- Sulman, B.N., Moore, J.A.M., Abramoff, R., Averill, C., Kivlin, S., Georgiou, K., Sridhar, B., Hartman, M.D., Wang, G., Wieder, W.R., Bradford, M.A., Luo, Y., Mayes, M.A., Morrison, E., Riley, W.J., Salazar, A., Schimel, J.P., Tang, J., Classen, A. T., 2018. Multiple models and experiments underscore large uncertainty in soil carbon dynamics. *Biogeochemistry* 141, 109–123.
- ter Braak, C.J.F., Vrugt, J.A., 2008. Differential Evolution Markov chain with snooker updaters and fewer chains. *Statistics and Computing* 18, 435–446.
- Viscarra Rossel, R.A., Lee, J., Behrens, T., Luo, Z., Baldock, J., Richards, A., 2019. Continental-scale soil carbon composition and vulnerability modulated by regional environmental controls. *Nature Geoscience* 12, 547–552.
- Vrugt, J.A., ter Braak, C.J.F., 2011. DREAM_(D): an adaptive Markov chain Monte Carlo simulation algorithm to solve discrete, noncontinuous, and combinatorial posterior parameter estimation problems. *Hydrology and Earth System Sciences* 15, 3701–3713.
- Waring, B.G., Sulman, B.N., Reed, S., Smith, A.P., Averill, C., Creamer, C.A., Cusack, D.F., Hall, S.J., Jastrow, J.D., Jilling, A., Kemner, K.M., Kleber, M., Liu, X.-J.A., Pett-Ridge, J., Schulz, M., 2020. From pools to flow: the PROMISE framework for new insights on soil carbon cycling in a changing world. *Global Change Biology* 26, 6631–6643.
- Wieder, W., Grandy, A., Kallenbach, C., Bonan, G., 2014. Integrating microbial physiology and physio-chemical principles in soils with the Microbial-Mineral Carbon Stabilization (MIMICS) model. *Biogeosciences* 11, 3899–3917.
- Wiesmeier, M., Lungu, M., Cerbari, V., Boincean, B., Hübler, R., Kögel-Knabner, I., 2018. Rebuilding soil carbon in degraded steppe soils of Eastern Europe: the importance of windbreaks and improved cropland management. *Land Degradation & Development* 29, 875–883.
- Wiesmeier, M., Urbanski, L., Hobley, E., Lang, B., von Lutzow, M., Marin-Spiotta, E., van Wesemael, B., Rabot, E., Liess, M., Garcia-Franco, N., Wollschlager, U., Vogel, H.J., Kögel-Knabner, I., 2019. Soil organic carbon storage as a key function of soils - a review of drivers and indicators at various scales. *Geoderma* 333, 149–162.
- Zimmermann, M., Leifeld, J., Schmidt, M.W.I., Smith, P., Fuhrer, J., 2007. Measured soil organic matter fractions can be related to pools in the RothC model. *European Journal of Soil Science* 58, 658–667.

Particulate and mineral-associated organic carbon turnover revealed by modelling their long-term dynamics

Guo, Xiaowei; Viscarra Rossel, Raphael A.; Wang, Guocheng; Xiao, Liujun; Wang, Mingming; Zhang, Shuai; Luo, Zhongkui

01 mingxi zhang

Page 1

7/2/2024 2:58

02 mingxi zhang

Page 2

7/2/2024 2:58

03 mingxi zhang

Page 2

5/2/2024 8:04

04 mingxi zhang

Page 8

5/2/2024 7:50

05 mingxi zhang

Page 8

5/2/2024 7:50

06 mingxi zhang

Page 9

7/11/2024 6:45